

Approximate Invariance of Metabolic Energy per Synapse during Development in Mammalian Brains

Jan Karbowski*

Institute of Biocybernetics and Biomedical Engineering, Polish Academy of Sciences, Warsaw, Poland

Abstract

During mammalian development the cerebral metabolic rate correlates qualitatively with synaptogenesis, and both often exhibit bimodal temporal profiles. Despite these non-monotonic dependencies, it is found based on empirical data for different mammals that regional metabolic rate per synapse is approximately conserved from birth to adulthood for a given species (with a slight deviation from this constancy for human visual and temporal cortices during adolescence). A typical synapse uses about $(7 \pm 2) \cdot 10^3$ glucose molecules per second in primate cerebral cortex, and about five times of that amount in cat and rat visual cortices. A theoretical model for brain metabolic expenditure is used to estimate synaptic signaling and neural spiking activity during development. It is found that synaptic efficacy is generally inversely correlated with average firing rate, and, additionally, synapses consume a bulk of metabolic energy, roughly 50–90% during most of the developmental process (except human temporal cortex < 50%). Overall, these results suggest a tight regulation of brain electrical and chemical activities during the formation and consolidation of neural connections. This presumably reflects strong energetic constraints on brain development.

Citation: Karbowski J (2012) Approximate Invariance of Metabolic Energy per Synapse during Development in Mammalian Brains. PLoS ONE 7(3): e33425. doi:10.1371/journal.pone.0033425

Editor: Mohammed Akaaboune, University of Michigan, United States of America

Received: December 22, 2011; **Accepted:** February 13, 2012; **Published:** March 27, 2012

Copyright: © 2012 Jan Karbowski. This is an open-access article distributed under the terms of the Creative Commons Attribution License, which permits unrestricted use, distribution, and reproduction in any medium, provided the original author and source are credited.

Funding: The work was supported by the grant from the Polish Ministry of Science and Education (NN 518 409238), and by the Marie Curie Actions EU grant FP7-PEOPLE-2007-IRG-210538. The funders had no role in study design, data collection and analysis, decision to publish, or preparation of the manuscript.

Competing Interests: The author has declared that no competing interests exist.

* E-mail: jkarbowski@mimuw.edu.pl

Introduction

The proper functioning of neural circuits depends on their proper wiring [1,2,3,4,5,6,7]. The right connectivity diagram is achieved during development that is both genetically and activity driven [8,9,10], and which probably has been optimized in the long evolutionary process [11,12]. Despite the widespread application of recording, imaging and molecular techniques [13,14], along with modeling studies [2,15,16], it is fair to say that our understanding of brain connectivity development is still very limited, and mostly qualitative. Nevertheless, the formation of neural circuits is an important problem in neuroscience, as its understanding may shed some light on structural memory formation in the brain and various developmental disorders [17]. Moreover, synaptic development like every physical process requires some energy. A natural question is how much does it cost, and whether this cost changes during development. It is known that information processing in the brain is metabolically expensive [18,19,20]. Specifically, energy consumption in mammalian brains increases fast with brain size, far more than in the rest of the body [21].

The process of synaptogenesis, i.e. formation of synaptic connections, can be region specific and can have a complicated time-course, often bimodal with synaptic overproduction early in the development [22,23,24,25,26,27,28,29]. However, we do not know whether and how this process correlates with the activities of participating neurons. It is also unclear, to what extent the synaptogenesis is regulated metabolically, although some qualitative correlation between the two has been noted based on their temporal characteristics [29,30].

A couple of theoretical investigations estimated that synapses in the adult brain consume a significant portion of the overall metabolic rate [31,32]. However, in fact, cerebral metabolic rate CMR (glucose consumption rate) depends both on neural electric discharges and on synaptic signaling, and their relative contribution is strongly controlled by a neurotransmitter release probability and synaptic density [33]. For instance, a high release probability can make synapses the major consumer of energy, and conversely, a low probability can cause action potentials to be metabolically dominant. Thus, simultaneous analysis of the cerebral metabolic rate and synaptic density during development can provide a useful quantitative information about the relative importance of these two factors. Additionally, it can yield a relationship between synaptic signaling and neural firing rates.

The main aim of this study is to address these questions in two steps. First, by collecting and analyzing empirical data on brain metabolism and synaptic density during development for different mammals. Second, by combining these data with a theoretical model for brain metabolic rate [33], in order to obtain quantitative results on the relationship energy vs. synapses. In particular, we want to establish how common across mammals are mechanisms that relate synaptogenesis with neural activities and cerebral metabolism. A secondary goal is to test the analytic model of brain metabolism against the data, which is a little extended here from its original formulation in [33]. In this model, cerebral metabolic rate is expressed solely by neural and synaptic physiological parameters that are either known or can be easily measured.

Table 1. Synaptic and metabolic development for rat and cat cerebral cortex.

Species/region	developmental	ρ_s	CMR	CMR/ ρ_s	η
	time	[10^{11} cm^{-3}]	$\left[\frac{\mu\text{mol}}{\text{g min}} \right]$	$\left[10^{-11} \frac{\mu\text{mol}}{\text{min}} \right]$	
Rat:					
parietal cortex	14 day	2.8 [22]	0.30 [34]	0.107	0.52
	17 day	6.3 [22]	0.42 [34]	0.067	0.84
	21 day	9.0 [22]	0.66 [34]	0.073	0.77
	35 day	14.0 [22]	0.85 [34]	0.061	0.92
	adult	13.5 [22]	0.94 [34]	0.070	0.81
Rat:					
visual cortex	10 day	0.62 [23]	0.20 [34]	0.323	0.10
	14 day	1.16 [23]	0.24 [34]	0.207	0.29
	17 day	2.68 [23]	0.32 [34]	0.119	1.19
	21 day	2.80 [23]	0.63 [34]	0.225	0.66
	35 day	3.00 [23]	0.87 [34]	0.290	0.55
	adult	2.95 [23]	0.97 [34]	0.329	0.48
Cat:					
visual cortex	1 day	0.20 [24]	0.318 [35]	1.590	0.08
	7 day	0.50 [24]	0.187 [35]	0.374	0.42
	30 day (est)	2.50 [24]	0.696 [35]	0.278	0.89
	40–45 day	3.10 [24]	0.987 [35]	0.318	0.83
	60–70 day	3.70 [24]	1.406 [35]	0.380	0.73
	110–120 day	3.10 [24]	1.201 [35]	0.387	0.68
	adult	2.70 [24]	1.120 [35]	0.415	0.61

Developmental time refers to postnatal time. References in the brackets. Synaptic contribution η to CMR is computed from Eq. (2).
doi:10.1371/journal.pone.0033425.t001

Table 2. Synaptic and metabolic development for monkey cerebral cortex.

Species/region	developmental	ρ_s	CMR	CMR/ ρ_s	η
	time	[10^{11} cm^{-3}]	$\left[\frac{\mu\text{mol}}{\text{g min}} \right]$	$\left[10^{-11} \frac{\mu\text{mol}}{\text{min}} \right]$	
Monkey:					
frontal cortex	2–3 month	6.0 [26]	0.33 [36]	0.055	0.63
	4–5 month	6.1 [26]	0.40 [36]	0.066	0.53
	6–7 month	5.7 [26]	0.39 [36]	0.068	0.49
	6 year	5.0 [26]	0.34 [38]	0.068	0.47
	20 y (adult)	3.16 [26]	0.22 [38]	0.070	0.36
Monkey:					
visual cortex	0–2 month	5.5 [25]	0.21 [37]	0.038	1.08
	2–6 month	9.0 [25]	0.50 [37]	0.056	0.94
	8–9 month	8.0 [25]	0.46 [36]	0.058	0.86
	12 month	6.0 [25]	0.33 [36]	0.055	0.78
	6–7 year	6.0 [25]	0.40 [38]	0.067	0.65
	20 y (adult)	3.8 [25]	0.27 [38]	0.071	0.49
Monkey:					
sensorimotor crt x	0–2 month	4.78 [27,28]	0.26 [37]	0.054	1.20
	2–3 month	5.75 [27,28]	0.34 [36]	0.059	1.11
	4–5 month	5.44 [27,28]	0.44 [36]	0.081	0.81
	6–7 month	5.19 [27,28]	0.38 [36]	0.073	0.89
	12–13 month	5.78 [27,28]	0.37 [36]	0.064	1.03

Developmental time refers to postnatal time. References in the brackets. Synaptic densities for sensorimotor cortex are arithmetic means of values in motor and somatosensory cortices.
doi:10.1371/journal.pone.0033425.t002

Table 3. Synaptic and metabolic development for human cerebral cortex.

Species/region	developmental time	ρ_s [10^{11} cm^{-3}]	CMR [$\frac{\mu\text{mol}}{\text{g min}}$]	CMR/ ρ_s [$10^{-11} \frac{\mu\text{mol}}{\text{min}}$]	η
Human:					
frontal cortex	- (10-8) wbb(*)	0.22 [29]	0.07 [39]	0.318	0.005
	1 day	1.95 [29]	0.13 [39,30]	0.067	0.33
	40 day	1.12 [29]	0.08 [39]	0.071	0.16
	80–83 day	3.10 [29]	0.15 [39]	0.048	0.81
	1.17 year	3.79 [29]	0.26 [30]	0.069	0.74
	3.5 year	5.24 [29]	0.56 [30]	0.107	0.70
	12 year	4.69 [29]	0.44 [30]	0.093	0.70
	15 year	4.00 [29]	0.41 [30]	0.103	0.53
	adult	3.40 [29]	0.27 [30]	0.079	0.56
Human:					
visual cortex	- (10-8) wbb(*)	1.2 [29]	0.06 [39]	0.050	0.98
	1 day	2.6 [29]	0.18 [30]	0.069	0.71
	1 year	5.5 [29]	0.28 [30]	0.051	0.96
	1.5 year	4.9 [29]	0.32 [30]	0.065	0.75
	3.5 year	4.7 [29]	0.60 [30]	0.128	0.38
	12 year	3.6 [29]	0.45 [30]	0.125	0.39
	adult	3.1 [29]	0.27 [30]	0.087	0.56
Human:					
temporal cortex	- (10-8) wbb(*)	0.75 [29]	0.06 [39]	0.080	0.06
	1 day	2.94 [29]	0.09 [39]	0.031	0.41
	40 day	2.10 [29]	0.07 [39]	0.033	0.30
	80–83 day	4.70 [29]	0.16 [39]	0.034	0.51
	1.17 year	5.30 [29]	0.24 [30]	0.045	0.42
	3.5 year	5.57 [29]	0.52 [30]	0.093	0.21
	12 year	2.47 [29]	0.39 [30]	0.158	0.07
	15 year	3.89 [29]	0.36 [30]	0.093	0.17
	adult	2.90 [29]	0.24 [30]	0.083	0.15

(*) Negative value refers to the weeks before birth (wbb). Positive developmental times refer to postnatal time. References in the brackets.
doi:10.1371/journal.pone.0033425.t003

Results

Constancy of metabolic energy per synapse during development

Empirical data (Tables 1–3) were used to analyze the time course of synaptic density (ρ_s) and glucose cerebral metabolic rate (CMR) during development for different mammals and brain regions (Fig. 1). For most regions both of these quantities depend non-monotonically on time, initially increasing, then reaching a maximum, and finally decreasing to adult values. In some cases, this temporal dependence is even more irregular, with more than one maximum (e.g. rhesus monkey frontal cortex and human temporal cortex for synaptic density). Overall, CMR and ρ_s can change several-fold during development. The most extreme change is in the cat visual cortex, where ρ_s and CMR can increase by a factor of ~ 18 and ~ 4 , respectively (Table 1). However, despite these complex dependencies and variability the amount of metabolic energy per synapse, i.e. the ratio CMR/ ρ_s , is nearly independent of the developmental time for a given species and brain area (Fig. 2; Tables 1–3). In all examined mammals and

cortical regions, the quantity CMR/ ρ_s correlates weakly with the developmental time, and the linear slope in this dependence is close to zero. Moreover, these weak correlations are not statistically significant (p value varies from 0.08 to 0.68; Fig. 2).

On average, rat brain consumes about $7 \cdot 10^{-13}$ μmol of glucose per minute per synapse in the parietal cortex, and $(2-3) \cdot 10^{-12}$ $\mu\text{mol}/\text{min}$ in the visual cortex (Table 1). The latter value is similar to the glucose use per synapse in the cat visual cortex (Table 1). In rhesus monkey and human cerebral cortices, there are approximately the same average baseline glucose consumptions per synapse, $\sim 7 \cdot 10^{-13}$ $\mu\text{mol}/\text{min}$ (Tables 2 and 3). From these results it follows that glucose use per synapse is smaller in large primate brains than it is in relatively small rodent or feline brains, and the difference could be five- or six-fold.

The biggest deviations from a baseline value of CMR/ ρ_s are for the human visual and temporal cortices between postnatal ages 3.5 and 12–15 years, and can be 2–3 folds above that baseline (Table 3). These numbers, however, do not seem to be relatively large, considering that CMR in that period can increase by a factor of 4–9 in relation to the minimal CMR. Nevertheless, the

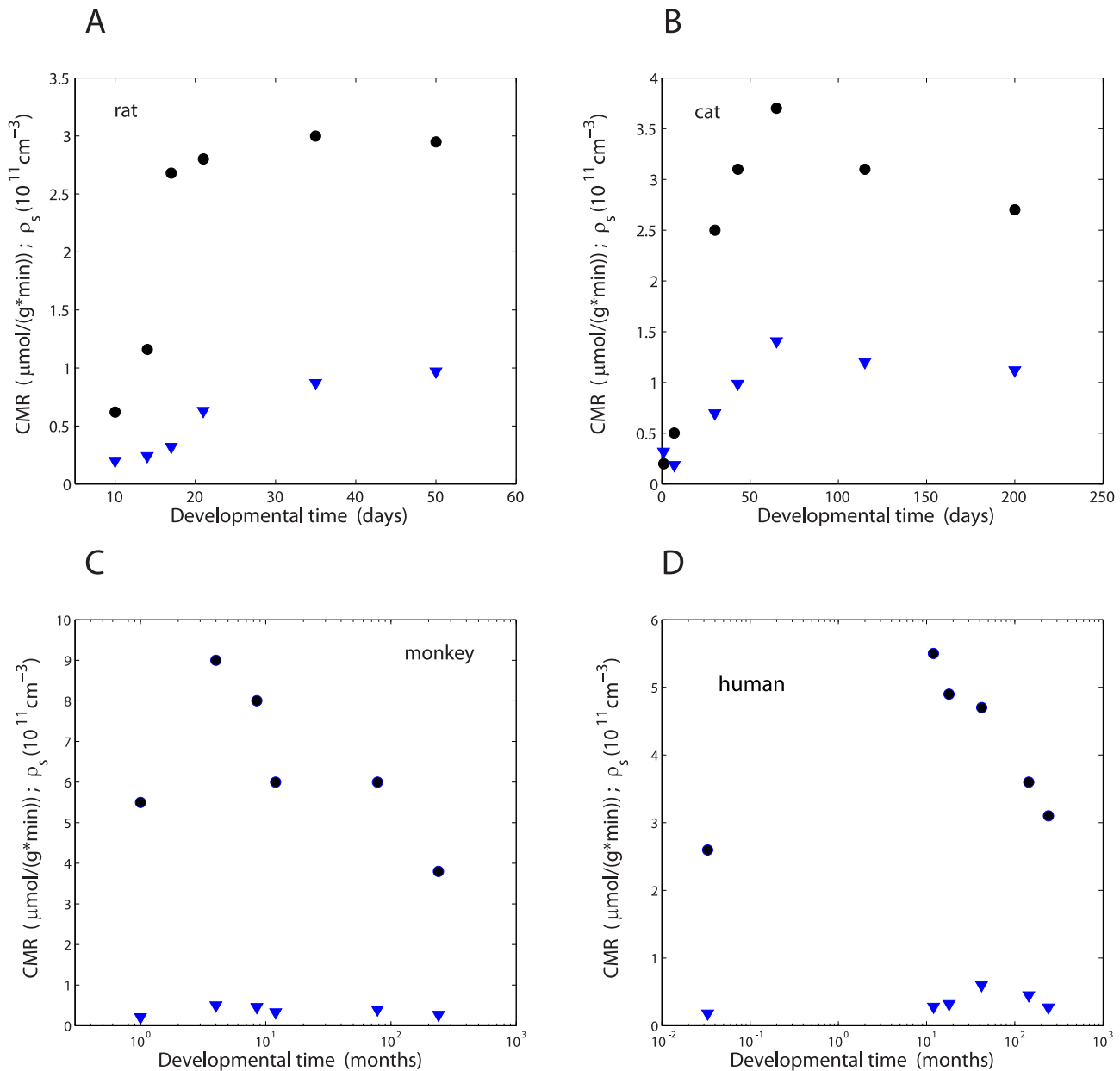


Figure 1. Dependence of glucose cerebral metabolic rate CMR and synaptic density ρ_s on developmental time in visual cortex of various mammals. (A) Rat; (B) Cat; (C) Monkey; (D) Human. Circles correspond to the synaptic density and triangles to CMR. doi:10.1371/journal.pone.0033425.g001

“energy per synapse” distinction for the (pre- and) adolescent human brain is noticeable and could suggest a different distribution of energy in the developing human neural circuits in that period in comparison to other mammals.

Correlation between cerebral metabolic rate and synaptic density

Empirical data on CMR and ρ_s were used to find their mutual relationship (Fig. 3). This relationship is in general monotonic with high positive correlations, and can be fitted by the formula, which was derived in the Materials and Methods:

$$\text{CMR} = a_0 + [a_1 + b\bar{\rho}_s]f(\bar{\rho}_s), \quad (1)$$

where a_0 and a_1 are numerical coefficients that depend on neurophysiological parameters (they are known and determined in the Materials and Methods), b is the parameter related to synaptic signaling, $\bar{\rho}_s$ is the amplitude of synaptic density, i.e. $\rho_s = \bar{\rho}_s 10^{11} [\text{cm}^{-3}]$. The function $f(\bar{\rho}_s)$ is the population average neural firing rate that changes during development with synaptic density as $f(\bar{\rho}_s) = f_0 \bar{\rho}_s^c$. Values of the parameters b , f_0 , and c are determined by a fitting procedure to the data, and they are presented in Table 4.

Generally, estimated average firing rates are rather small for all examined mammals, and on average about 1 Hz (Table 4). The smallest values are for the monkey visual and sensorimotor cortices, and the largest for the cat visual cortex. The character of the relationship between population firing rate f and synaptic

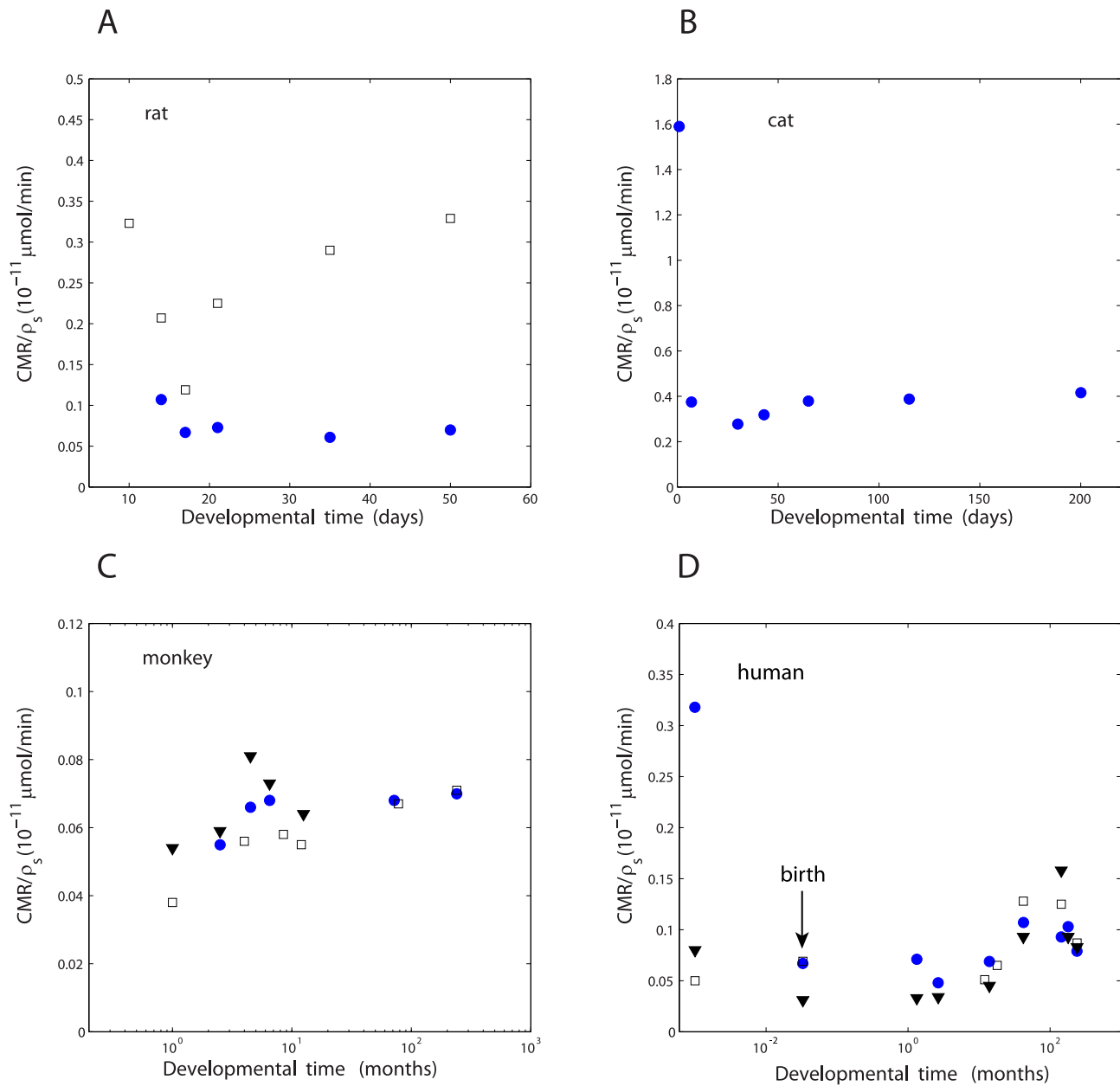


Figure 2. Approximate invariance of glucose cerebral metabolic rate per synapse during development. The linear fits to the data points are given in the brackets below. (A) Rat (circles - parietal cortex: $y = -0.0006x + 0.092$, $R^2 = 0.259$, $p = 0.381$; squares - visual cortex: $y = 0.0025x + 0.187$, $R^2 = 0.223$, $p = 0.345$). (B) Cat visual cortex (with the data point at 1 day: $y = -0.0023x + 0.684$, $R^2 = 0.118$, $p = 0.451$; without the data point at 1 day: $y = 0.00003x + 0.063$, $R^2 = 0.279$, $p = 0.363$; squares - visual cortex: $y = 0.00009x + 0.052$, $R^2 = 0.527$, $p = 0.102$; triangles - sensorimotor cortex: $y = 0.0007x + 0.063$, $R^2 = 0.075$, $p = 0.656$). (C) Monkey (circles - frontal cortex: $y = 0.00009x + 0.052$, $R^2 = 0.527$, $p = 0.102$; squares - visual cortex: $y = 0.00009x + 0.052$, $R^2 = 0.527$, $p = 0.102$; triangles - sensorimotor cortex: $y = 0.0007x + 0.063$, $R^2 = 0.075$, $p = 0.656$). (D) Human (circles - frontal cortex: $y = -0.0001x + 0.116$, $R^2 = 0.025$, $p = 0.684$; squares - visual cortex: $y = 0.0002x + 0.071$, $R^2 = 0.223$, $p = 0.282$; triangles - temporal cortex: $y = 0.0003x + 0.053$, $R^2 = 0.375$, $p = 0.079$). In the above fits y refers to CMR/ρ_s (in $10^{-11} \mu\text{mol}/\text{min}$) and x to the developmental time (either in days for rat and cat or in months for monkey and human). Note that for all fits the linear coefficient is close to zero. doi:10.1371/journal.pone.0033425.g002

density ρ_s is not universal, but depends on a particular species and cortical region (Table 4). For some regions, the best fit is obtained for f independent of ρ_s (i.e. with $c \approx 0$). For others, we find an increase of f with increasing ρ_s , either sublinearly ($c < 1$) or approximately linearly ($c \approx 1$). The nature of this dependence has also its influence on the relationship CMR vs. ρ_s . When $c > 0$, that is, when f increases with ρ_s , we find that CMR increases with ρ_s in a non-linear manner (Fig. 3B,C,D), whereas when $c = 0$, then

CMR grows linearly with ρ_s (Fig. 3A). Thus, we conclude that the dependence CMR on ρ_s is also non-universal.

Synaptic contribution to the cerebral metabolic rate during development

Having determined the parameters b , f_0 , and c , we can find a fraction of metabolic energy consumed by synaptic signaling

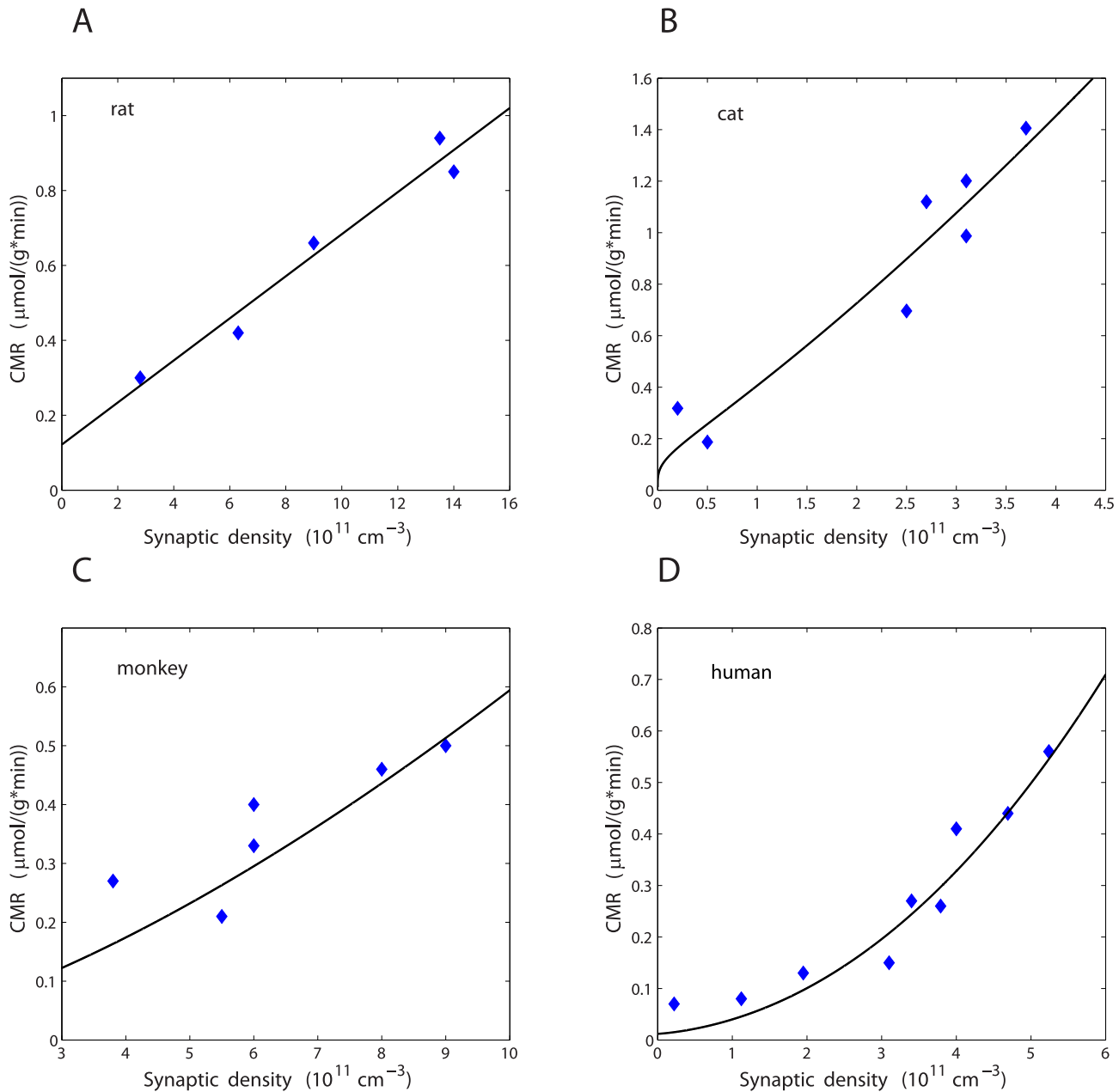


Figure 3. Empirical dependence of cerebral metabolic rate CMR on synaptic density ρ_s together with fits to the theoretical metabolic model. (A) Rat, parietal cortex. (B) Cat, visual cortex. (C) Monkey, visual cortex. (D) Human, frontal cortex. Empirical data are represented by diamonds, and theoretical fits by solid lines. The fitting parameters are shown in Table 4.
doi:10.1371/journal.pone.0033425.g003

during the development process. The fraction η of the cerebral metabolic rate CMR taken by synapses is defined as $\eta = b\bar{\rho}_s f(\bar{\rho}_s) / CMR$, or equivalently

$$\eta = \frac{bf}{CMR/\bar{\rho}_s}. \quad (2)$$

The latter expression implies that η is inversely related to the metabolic energy per synapse. Indeed, although η changes during the development much more than $CMR/\bar{\rho}_s$ (Tables 1–3), both of these variables are negatively correlated (Table 5). The greater

variability of η than $CMR/\bar{\rho}_s$ can be explained by its additional dependence on firing rate $f(\bar{\rho}_s)$, which in itself is proportional to a variable synaptic density.

In general, η is rather high, mostly in the range 0.5–0.9 (Tables 1–3; some η is a little above unity, which is an artifact caused by systematic errors in the fitting procedure that determines b , c , and f_0). A significant exception is human temporal cortex in which synapses use for the most time considerably less than 50% of cortical CMR. At the top of the synaptogenesis, when synaptic density is maximal, η is usually very large and often around 0.8–0.9, which is greater than for the adult, but the difference is mild. From all examined mammals and cortical regions, synapses in the monkey visual and sensorimotor

Table 4. Best fits to the data for parameters in the relation CMR vs. ρ_s across mammals.

Species/region	b ($\mu\text{mol} \cdot \text{s}/\text{min}$)	c	f_0 (Hz)	f (Hz)	R^2	SSE
Rat: parietal cortex	0.066	0.0	0.85	0.85	0.961	0.012
Rat: visual cortex	0.071	1.02	0.73	0.4–2.2	0.674	0.181
Cat: visual cortex	0.121	0.29	1.57	1.0–2.3	0.905	0.121
Monkey: frontal cortex	0.024	0.52	0.57	1.0–1.5	0.776	0.011
Monkey: visual cortex	0.228	0.48	0.08	0.15–0.23	0.908	0.005
Monkey: sensorimotor crtx	0.692	0.03	0.09	0.1	0.262	0.013
Human: frontal cortex	0.070	1.23	0.14	0.02–1.1	0.928	0.018
Human: visual cortex	0.038	0.0	1.29	1.3	0.105	0.127
Human: temporal cortex	0.010	0.69	0.60	0.5–2.0	0.347	0.142

doi:10.1371/journal.pone.0033425.t004

cortices, as well as synapses in the rat parietal cortex seem to be the most “energetic”, since they frequently use approximately 90% of the total cerebral glucose rate.

Overall, these results strongly suggest that excitatory synaptic signaling uses a majority of metabolic energy allocated to neurons, even at adulthood. The spiking neural activity and maintenance of negative membrane potential utilize generally far less energy, together approximately 10–40%, depending on the species, brain region, and developmental period.

Relationship between synaptic efficacy and average firing rate across mammals

The parameter b in Eq. (1) is proportional to the excitatory synaptic efficacy (or signaling; see Materials and Methods). For a given species, we can associate this parameter with the average firing rate f , both of which were determined by fitting the theoretical model (Eq. 1) to the data (Table 4). We find that b and f are inversely correlated across all examined cerebral regions and animals, and can be fitted quite well by a universal curve of the form ($R^2 = 0.956$; Fig. 4):

$$b = 0.03f^{-1.35}, \quad (3)$$

where b is expressed in $\mu\text{mol} \cdot \text{sec}/\text{min}$. This relationship indicates that average synaptic efficacy is dependent on network spiking activity, and the higher that activity the smaller synaptic signaling. For example, for $f = 0.1$ Hz we have $b \approx 0.7$, while for $f = 1.3$ Hz we obtain $b \approx 0.03$, i.e. more than twenty-fold reduced synaptic efficacy. This implies that synaptic transmission is very sensitive on the average firing rate in the network, which can have functional consequences (see Discussion).

Estimation of neurotransmitter release probability by combining data and metabolic model

Experimental data show that the probability of neurotransmitter release is the least stable parameter among synaptic parameters, and can change during the development by at least an order of magnitude [40,41]. To test our metabolic model (see Materials and Methods), the release probability is estimated below for adult rat and cat visual cortices. In this respect, we equate the empirical value of the parameter b in Table 4 with the analytical formula for b given by Eq. (15), which allows us to determine the release probability q . We assume that $\bar{g}_{AMPA}/\bar{g}_{NMDA} \approx 2.5$, in agreement

Table 5. Correlation between metabolic energy per synapse (CMR/ ρ_s) and synaptic fraction of metabolism (η).

Species/region	correlation	significance
	r	p
Rat: parietal cortex	−0.992	0.001
Rat: visual cortex	−0.753	0.084
Cat: visual cortex	−0.869	0.011
Monkey: frontal cortex	−0.889	0.044
Monkey: visual cortex	−0.927	0.008
Monkey: sensorimotor crtx	−0.995	0.000
Human: frontal cortex	−0.642 (0.049)	0.063 (0.908)
Human: visual cortex	−0.968 (−0.968)	0.000 (0.002)
Human: temporal cortex	−0.659 (−0.872)	0.054 (0.005)

Values in the brackets refer to r and p without the prenatal data points.
doi:10.1371/journal.pone.0033425.t005

with the empirical data for adult primate brain [42]. We take the peak AMPA synaptic conductances and their decay time constants as: $\bar{g}_{AMPA} = 3.6 \cdot 10^{-10} \Omega^{-1}$ and $\tau_{AMPA} = 5 \cdot 10^{-3}$ s for rat, and $\bar{g}_{AMPA} = 7.1 \cdot 10^{-10} \Omega^{-1}$ and $\tau_{AMPA} = 7.6 \cdot 10^{-3}$ s for cat [43]. Additionally, the NMDA synaptic conductance decay time constant τ_{NMDA} is taken as $\tau_{NMDA} = 0.1$ s for both species, as a standard NMDA decay time [44]. We find that the neurotransmitter release probability q is 0.45 for adult rat visual cortex, and 0.31 for adult cat visual cortex. These values are in the range of values reported experimentally [40,45,46], and suggest that the metabolic model presented and used in this paper (Materials and Methods) is reliable and has a predictive power.

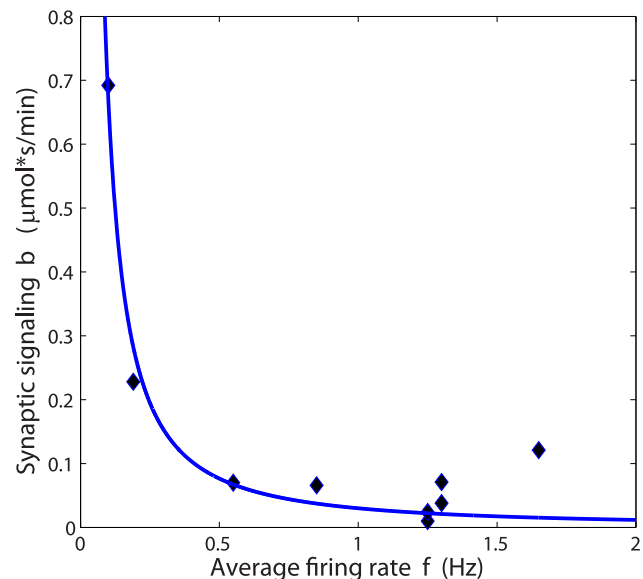


Figure 4. Inverse relationship between synaptic signaling and average firing rate across mammals. Values of the synaptic efficacy b and firing rates f (arithmetic means) were found by fitting experimental data to the theoretical model (Table 4). Note that all data points (diamonds) coming from different species and cortical regions align into a universal curve of the form: $b = 0.03f^{-1.35}$ ($R^2 = 0.956$, $p < 0.001$).

doi:10.1371/journal.pone.0033425.g004

Discussion

This study shows that despite temporal changes in cerebral metabolic rate CMR and synaptic density ρ_s during development, often exhibiting bimodal shape, the amount of metabolic energy per synapse (CMR/ρ_s) is almost invariant in the process for a given mammal and brain region (Fig. 2; Tables 1–3). This approximate constancy is even more pronounced if we take into account that many other neuroanatomical parameters, such as neuron number, dendritic tree length, and brain volume, all change non-monotonically with an animal age [47,48,49]. In contrast to CMR/ρ_s , the fraction of CMR consumed by synapses, i.e. η , is much more variable during the development (Tables 1–3). Moreover, these two quantities are strongly negatively correlated (Table 5). For the most developmental time and cortical regions η is greater than 0.5, implying that synapses use the majority of cortical metabolic energy, often close to 90% or more (Tables 1–3).

The case with the human brain is more subtle, as its visual and temporal cortices exhibit a noticeable deviation from the CMR/ρ_s constancy during early and middle adolescence (by a factor of ~ 2 ; Table 3). In addition, η for human temporal cortex is considerably smaller than 0.5 for the most time. The increase in CMR/ρ_s for the above regions during adolescence is associated with a simultaneous decrease in η , which suggests that non-synaptic part of CMR dominates over the synaptic part in this period (Table 3). It is interesting to note that the maxima of CMR/ρ_s for human visual and temporal cortices between 3.5 and 12 years coincide with maxima observed in cortical volume, thickness, and surface area during the same time [50,51,52]. This positive (negative) correlation between CMR/ρ_s (η) and structural cortical growth can be an indication that the latter process requires an additional energy above some baseline, which is partly generated by shunting it from the synapses.

On average, a synapse in the primate cerebral cortex consumes about $(7 \pm 2) \cdot 10^{-13}$ μmol of glucose per minute. In rat and cat visual cortices corresponding numbers are about 5 times larger, which qualitatively agrees with a previous rough estimate that in larger brains energy per synapse should be smaller than in smaller brains [21]. These numbers translate into 5000–9000 of consumed glucose molecules and $(1.6–2.8) \cdot 10^5$ of consumed ATP molecules, both per second and per synapse in the primate cortex (using Avogadro number $\approx 6 \cdot 10^{23}$ mol^{-1} , and the fact that about 31 ATP molecules are produced per one used glucose molecule [53]). Thus, the cost of creating and maintaining one synapse in the human cortex during development is about $2.2 \cdot 10^5$ ATP molecules/second, which can increase during adolescence to $4 \cdot 10^5$ ATP/sec.

There is a growing evidence that a typical excitatory synapse can operate only in a limited number of structurally different discrete states [54,55]. Since the sizes of synapses (lengths of postsynaptic densities) during postnatal development remain roughly constant [23,28], one can assume that the number of synaptic states is also approximately invariant. Assuming that a synapse has on average between 10 and 100 states [55], we can estimate the amount of ATP utilization per 1 bit of stored synaptic information. For human brain we obtain $2.2 \cdot 10^5 / \log_2 10^n \sim (3–6) \cdot 10^4$ ATP/bit per second, where $n=1$ or 2. Thus, during a human lifetime (~ 80 years) a typical synapse uses $(3 \pm 1) \cdot 10^{14}$ ATP molecules per stored 1 bit of information.

Invariants in the brain design or dynamics are not too numerous, and their existence clearly deserves more attention and thought. The current finding about the constant energy per synapse during development (for a given brain region) expands a short list of the discovered invariants, including adult synaptic

density across mammals [56,57], volume-specific metabolic scaling exponent across gray matter (≈ -0.15) [21], energy per neuron across mammals [58,59], blood flow and capillary length per neuron [59], or fraction of brain volume taken by glia across mammals [60,61]. It seems that there are some common principles underlying these invariants, which could be related to the economy of brain wiring [3,4,5,62,63,64,65]. This in turn could be associated with the evolutionary constraints coming from limited energetic resources [19,20,31], as the brain is an energy-expensive organ [18,21], and synapses were pointed out as one of the important users of the cerebral metabolism [21,31,32,33]. The fact that cerebral metabolic rate CMR and synaptic density ρ_s are rather strongly positively correlated (Table 4, Fig. 3) speaks in support of the last argument.

The results in this study indicate that synapses are even bigger energy users than previously estimated. Calculations presented in Tables 1–3 show that at adulthood, when synaptic density is generally lower than in adolescence, synapses can still consume about 50–80% of the total glucose consumption rate. For example, for rat cortex η is either 0.48 (visual) or 0.81 (parietal). The average of these values is about twice the amount that was previously calculated for adult rat cortex [31]. The likely source of the discrepancy is the probability of neurotransmitter release, which was calculated here as 0.45 (for rat visual cortex), and assumed in [31] as 0.25. Generally, it should be kept in mind that the computed values of the release probability are only averages, as this parameter is highly variable in time and additionally input specific, and could be somewhere between 0.05–0.7 [40,41,45,46]. Because the neurophysiological model of the gray matter metabolism presented in this paper (see Materials and Methods) yields reasonable numerical values of this highly uncertain parameter, it could play a useful role in the future in determining other functional circuit parameters from glucose metabolic data.

It is found that, as a rule, synaptic efficacy (signaling) is negatively correlated with cortical average neural firing rate across all examined species (Fig. 4). Low firing rates usually correspond to high synaptic efficacy, and vice versa (Fig. 4). The interesting feature is that all data points coming from different mammals and cortical regions collapse (with high correlations) into one universal curve given by Eq. (3). This clearly suggests that synaptic regulatory mechanisms such as depression and potentiation are coupled with global network activity and may have a universal cross-species character. This kind of synaptic plasticity is reminiscent of the so-called synaptic scaling, which was found in cortical circuits [66]. In this process, which is typically slow, synaptic efficacy increases if network activity is too low, and it decreases if network activity is too high. This synapse-network activity coupling serves as a tuning mechanism to balance brain spiking activity, which may be important for preventing pathological dynamic states [67].

The collected empirical data in combination with the theoretical metabolic model allow us to determine average firing rates across mammals during development, from the birth to adulthood. These rates are rather low, generally in the range 0–2.3 Hz. This probably implies that only a small fraction of cells is active concurrently, which is compatible with an idea of sparse neural coding in cortical networks [19,31]. Moreover, our results show that larger brains tend to have a slightly lower spiking activities than smaller brains (Table 4). This conclusion that was reached here for developing brains is in line with a previous estimate made for several adult mammals, also using glucose metabolic data [33]. The current interesting finding is that neural firing rate could change during development in coordination with the changes in

synaptic density (Table 4). Such dependence improves the goodness of fits for several brain regions significantly.

The semi-empirical results of this study can have some impact on modeling studies related to the connectivity development in the brain. It has been known for a long time that synaptic development is driven to some extent by global spiking activity of neurons [14,68]. This coupling has also been incorporated in several formal models dealing with synaptogenesis [16,69], but it often had abstract forms. It seems that the semi-empirical formula derived here (Eq. 3), allows us for a more realistic approach. Alternatively, this formula could be used as a one of the criteria for verification of modeling studies. Similarly, the finding that there exist a (roughly) constant amount of available energy per synapse during development (Fig. 2; Tables 1–3), has not been explored in computational models. Yet, it could have important theoretical implications.

Although, the empirical data in this paper are concerned with normal development, they could also have some relevance for studies dealing with developmental disorders, such as schizophrenia or autism. There are some strong experimental indications that these mental diseases are associated with altered synaptic connectivity [70,71]. It would be interesting to know whether in these disorders the amount of metabolic energy per synapse during development is also conserved or not? If not, then how large are deviations from a constancy, and whether this measure is somehow correlated with the degree of mental disorder. This perhaps could have some practical applications.

Materials and Methods

Developmental data

The ethics statement does not apply to this study. Experimental data for glucose cerebral metabolic rate (CMR) and synaptic density (ρ_s) during development for rat, cat, macaque monkey, and human are presented in Tables 1–3. These mammals have adult brains that span 3 orders of magnitude in volume. The metabolic data were collected from the following sources: for rat [34]; for cat [35]; for monkey [36,37,38]; for human [30,39]. The synaptogenesis data were taken from: [22,23] for rat; [24] for cat; [25,26,27,28] for monkey; and [29] for human.

Theoretical model of cerebral metabolic rate

In this section we derive an expression for the glucose cerebral metabolic rate CMR in gray matter. This derivation follows closely a detailed analysis presented in [33], and additionally extends it by including also NMDA synaptic currents. We assume that the activities of Na^+/K^+ pumps are the major contributors to brain metabolism, which is in agreement with empirical estimates [72,73]. The main objective of these pumps is to remove Na^+ ions from neuron's interior, in order to maintain a negative membrane resting potential, which is critical for all neural functions.

During one cycle, the Na^+/K^+ pump extrudes 3 Na^+ and intrudes 2 K^+ ions, which translates into a net removal of one elementary positive charge that comprises a pump current I_p . Consequently, the pump current I_p constitutes of only 1/3 of the total sodium current through the membrane. In terms of the metabolic cost, this pumping process uses 1 ATP molecule (per one cycle) to remove one positive charge. The metabolic expenditure of this process in the long run depends on the level of intracellular sodium concentration.

According to biochemical estimates [53], about 31 ATP molecules are made per one oxidized glucose molecule during

cellular respiration. Consequently, the glucose metabolic rate CMR (the amount of moles of glucose per tissue volume and time) is given by

$$\text{CMR} = \frac{N\bar{I}_p}{31UF}, \quad (4)$$

where \bar{I}_p is the average net pump current, N is the number of neurons contained in the gray matter volume U , and F is the Faraday constant. The ratio \bar{I}_p/F is the amount of moles of ATP molecules consumed on average per neuron per time unit.

At the steady state, i.e. for constant firing rates and after averaging over long times (hundred of seconds to several minutes), the average sodium concentration inside neurons is relatively stable [33]. This corresponds to the situation when the pump current \bar{I}_p balances 3 different types of sodium currents through the membrane [33]:

$$3\bar{I}_p = I_{Na,0} + I_{ap} + I_{s,0}, \quad (5)$$

where $3\bar{I}_p$ is the amount of Na^+ charge per second that is removed by the Na^+/K^+ pump. The current $I_{Na,0}$ is Na^+ influx through sodium channels at rest (a small contribution), I_{ap} is Na^+ influx due to action potentials, and $I_{s,0}$ is the sodium influx through synapses during background dendritic synaptic activity. The explicit forms of the first two currents are given by:

$$I_{Na,0} = g_{Na,0}S(V_{Na} - V_0), \quad (6)$$

$$I_{ap} = f\bar{C}S(V_{Na} - V_0), \quad (7)$$

where V_{Na} is the reversal potential for Na^+ ions, V_0 is the resting membrane potential, f is the average firing rate, $g_{Na,0}$ is the resting Na^+ conductance per unit area, \bar{C} is effective membrane capacitance per unit area, and S is the neuron's membrane surface area.

The synaptic contribution $I_{s,0}$ to the sodium influx is proportional to a temporal average over an interspike interval of the AMPA and NMDA synaptic currents, and takes the form:

$$I_{s,0} = \alpha M f q \int_0^{1/f} dt [g_{AMPA}(t) + G(V)g_{NMDA}(t)]V, \quad (8)$$

where α is the proportionality factor between the total synaptic current and Na^+ influx current and is given by $\alpha = V_K(V_{Na} - V_0)/[V_0(V_K - V_{Na})]$, where V_K is the reversal potential for K^+ ions. The latter dependence can be easily computed [33] and follows from the fact that AMPA current is composed exclusively of Na^+ and K^+ ions, and NMDA current is composed largely of these ions (the influence of Ca^{+2} is neglected here, as it constitutes only of about 7–10% of the NMDA current [74]). The symbol M denotes number of synapses per neuron, q is the neurotransmitter release probability, and V is neuron's membrane voltage. The function $G(V)$ is a voltage-dependent factor associated with NMDA receptors given by [44]: $G(V) = 1/[1 + 0.33 \exp(-0.06V)]$, where V is in mV. For voltage equal to the resting potential, i.e. $V = V_0 = -65$ mV, we obtain $G_0 \equiv G(V_0) = 0.06$. The symbols $g_{AMPA}(t)$ and $g_{NMDA}(t)$ denote the time dependent single synapse conductances, respectively AMPA and NMDA type. Below, we assume that the rising phase of these conductances is much faster than their decaying

phases. That is, we take $g_{AMPA} = \bar{g}_{AMPA} \exp(-t/\tau_{AMPA})$, and $g_{NMDA} = \bar{g}_{NMDA} \exp(-t/\tau_{NMDA})$, where \bar{g}_{AMPA} , \bar{g}_{NMDA} are the peak conductances, and τ_{AMPA} , τ_{NMDA} are corresponding decay time constants. Also, since the duration of a single action potential is very short in comparison to the average interspike interval $1/f$, we can assume that for the most time $V \approx V_0$ under the integral. With these assumptions we can carry out the integration in Eq. (8), with the result

$$I_{s,0} = \frac{qfMV_K(V_{Na} - V_0)}{(V_K - V_{Na})} \quad (9)$$

$$[\bar{g}_{AMPA}\tau_{AMPA}R_{AMPA}(f) + G_0\bar{g}_{NMDA}\tau_{NMDA}R_{NMDA}(f)],$$

where the frequency dependent factor $R_i(f)$ ($i = AMPA, NMDA$) has the form: $R_i(f) = 1 - \exp[-1/(f\tau_i)]$. This factor for the AMPA current is practically always close to 1, as $f\tau_{AMPA}$ is significantly smaller than unity even for firing rates f as large as 100 Hz (with $\tau_{AMPA} \sim 5-6$ msec). Generally, for the NMDA current R_{NMDA} is less than 1, and could be even $\ll 1$ for very large f . However, for the empirical frequencies found in this study (~ 1 Hz), the factor $R_{NMDA} \approx 1$. Consequently, the values of R_{AMPA} and R_{NMDA} are both taken as 1 further in the analysis.

Combination of Eqs. (4–7) and (9) yields an approximate glucose metabolic rate CMR as follows:

$$CMR = \frac{NS(V_{Na} - V_0)}{U \cdot 93F} \quad (10)$$

$$\left[g_{Na,0} + f\bar{C} + \frac{M}{S} \frac{V_K qf}{(V_K - V_{Na})} (\bar{g}_{AMPA}\tau_{AMPA} + G_0\bar{g}_{NMDA}\tau_{NMDA}) \right].$$

Additionally, we assume that the geometry of axons and dendrites can be approximated as cylindrical with equal volumes [56]. Thus, we can write the total membrane surface area as $NS = 4(1-\phi)U/d$, where d is an effective fiber diameter (harmonic mean of axonal and dendritic diameters), and $(1-\phi)$ is the fraction of volume taken by neural wiring [33]. Moreover, the surface density of synapses can be written as $M/S = \rho_s d / (4(1-\phi))$, where ρ_s is the synaptic density [33]. Substituting the above expressions for NS/U and M/S into Eq. (10), we obtain CMR in a more convenient form:

$$CMR = \frac{(V_{Na} - V_0)}{93F} \quad (11)$$

$$\left[\frac{4(1-\phi)}{d} (g_{Na,0} + f\bar{C}) + \frac{qf\rho_s V_K}{(V_K - V_{Na})} (\bar{g}_{AMPA}\tau_{AMPA} + G_0\bar{g}_{NMDA}\tau_{NMDA}) \right],$$

or equivalently with an explicit dependence of CMR on synaptic density and firing rate as:

$$CMR = a_0 + a_1 f + b \bar{\rho}_s f, \quad (12)$$

where the coefficients a_0 , a_1 , and b are given by

$$a_0 = \frac{4(1-\phi)g_{Na,0}(V_{Na} - V_0)}{93Fd}, \quad (13)$$

$$a_1 = \frac{4(1-\phi)\bar{C}(V_{Na} - V_0)}{93Fd}, \quad (14)$$

and

$$b = \frac{10^{11} q V_K (V_{Na} - V_0) [\bar{g}_{AMPA} \tau_{AMPA} + G_0 \bar{g}_{NMDA} \tau_{NMDA}]}{93F (V_K - V_{Na})}. \quad (15)$$

In Eq. (12) the firing rate f is in Hz, and the symbol $\bar{\rho}_s$ denotes the synaptic density amplitude defined as $\bar{\rho}_s = \bar{\rho}_s 10^{11}$, where ρ_s is expressed in cm^{-3} . The coefficients a_0 and a_1 are invariant or nearly invariant across species, and they do not seem to change significantly during development after birth. This is because they depend on the parameters, which themselves are developmentally or species independent. These are electrical voltages (V_{Na} , V_K , V_0) due to their logarithmic dependencies on ionic concentrations, membrane capacity \bar{C} , and structural parameters: the fraction of volume taken by wiring $(1-\phi)$ or fraction of neuropil [26,27,28], and the effective wire thickness d [56]. Also the sodium conductance at neuron's rest is very small, and biophysical models suggest that it is similar across species. The numerical values of these parameters are: $V_{Na} = 0.050$ V, $V_K = -0.100$ V, $V_0 = -0.065$ V (standard values), $(1-\phi) \approx 0.65$ [26,27,28,56], $g_{Na,0} = 3 \cdot 10^{-7}$ (Ωcm^2) $^{-1}$ [33], $\bar{C} \approx 3.2 \cdot 10^{-6}$ F/cm 2 , and $d = 0.45 \cdot 10^{-4}$ cm [33]. Based on these values, we obtain $a_0 = 0.013$ $\mu\text{mol}/(\text{g}\cdot\text{min})$, and $a_1 = 0.14$ $\mu\text{mol}\cdot\text{s}/(\text{g}\cdot\text{min})$. The parameter b is related to synaptic activities, and its value is determined in the Results section for every species and brain region.

There are no data on *in vivo* firing rates during development. Therefore, we have to assume some form of f . We consider two scenarios for this quantity. In the simplest case, firing rate and synaptic density are independent of each other, and we take f to be a constant. In a second case, we assume that firing rate and synaptic density are correlated in such a way that f is an increasing function of $\bar{\rho}_s$. This follows from a simple expectation that higher synaptic density generally mean more excitatory synaptic input to a typical neuron, as 85% of synapses in the cerebral cortex are excitatory [56,57]. More excitatory input in a recurrent network translates into higher average firing rates. This is in agreement with mean-field models of recurrent neural networks [75]. Thus, the simplest expression for the firing that combines both scenarios is $f = f_0 \bar{\rho}_s^c$, where f_0 and the exponent c are to be determined by a fitting procedure to the data. When $c = 0$, then f is independent of synaptic density.

Author Contributions

Conceived and designed the experiments: JK. Performed the experiments: JK. Analyzed the data: JK. Contributed reagents/materials/analysis tools: JK. Wrote the paper: JK.

References

- Douglas RJ, Martin KA (2004) Neuronal circuits of the neocortex. *Annu Rev Neurosci* 27: 419–451.
- Chechik G, Meilijson I, Ruppin E (1999) Neuronal regulation: a mechanism for synaptic pruning during brain maturation. *Neural Comput* 11: 2061–2080.
- Kaas JH (2000) Why is brain size so important: Design problems and solutions as neocortex gets bigger or smaller. *Brain Mind* 1: 7–23.
- Karbowski J (2001) Optimal wiring principle and plateaus in the degree of separation for cortical neurons. *Phys Rev Lett* 86: 3674–3677.

5. Karbowski J (2003) How does connectivity between cortical areas depend on brain size? Implications for efficient computation. *J Comput Neurosci* 15: 347–356.
6. Laughlin SB, Sejnowski TJ (2003) Communication in neuronal networks. *Science* 301: 1870–1874.
7. Chklovskii DB (2004) Synaptic connectivity and neuronal morphology: two sides of the same coin. *Neuron* 43: 609–617.
8. Katz LC, Shatz CJ (1996) Synaptic activity and the construction of cortical circuits. *Science* 274: 1133–1138.
9. Cohen-Cory S (2002) The developing synapse: construction and modulation of synaptic structures and circuits. *Science* 298: 770–776.
10. Le Be JV, Markram H (2006) Spontaneous and evoked synaptic rewiring in the neonatal neocortex. *Proc Natl Acad Sci USA* 103: 13214–13219.
11. Allman JM (1999) *Evolving Brains*. New York: Freeman.
12. Striedter GF (2005) *Principles of brain evolution*. Sunderland, MA: Sinauer Assoc.
13. Silberberg G, Grillner S, LeBeau FEN, Maex R, Markram H (2005) Synaptic pathways in neural microcircuits. *Trends Neurosci* 28: 541–551.
14. Lendvai B, Stern EA, Chen B, Svoboda K (2000) Experience-dependent plasticity of dendritic spines in the developing rat barrel cortex in vivo. *Nature* 404: 876–881.
15. Karbowski J, Ermentrout GB (2004) Model of the early development of thalamo-cortical connections and area patterning via signaling molecules. *J Comput Neurosci* 17: 347–363.
16. *Modeling Neural development* (2003) Editor: van Ooyen A. The MIT Press, Cambridge, Massachusetts.
17. Rakic P, Bourgeois JP, Goldman-Rakic PS (1994) Synaptic development of the cerebral cortex: implications for learning, memory, and mental illness. *Prog Brain Res* 102: 227–243.
18. Aiello LC, Wheeler P (1995) The expensive-tissue hypothesis: The brain and the digestive-system in human and primate evolution. *Curr Anthropology* 36: 199–221.
19. Levy WB, Baxter RA (1996) Energy efficient neural codes. *Neural Comput* 8: 531–543.
20. Laughlin SB, de Ruyter van Steveninck RR, Anderson JC (1998) The metabolic cost of neural information. *Nature Neurosci* 1: 36–41.
21. Karbowski J (2007) Global and regional brain metabolic scaling and its functional consequences. *BMC Biology* 5: 18.
22. Aghajanian GK, Bloom FE (1967) The formation of synaptic junctions in developing rat brain: A quantitative electron microscopic study. *Brain Res* 6: 716–727.
23. Blue ME, Parnavelas JG (1983) The formation and maturation of synapses in the visual cortex of the rat. II. Quantitative analysis. *J Neurocytol* 12: 697–712.
24. Winfield DA (1981) The postnatal development of synapses in the visual cortex of the cat and the effects of eyelid closure. *Brain Res* 206: 166–171.
25. Bourgeois JP, Rakic P (1993) Changes of synaptic density in the primary visual cortex of the macaque monkey from fetal to adult stage. *J Neurosci* 13: 2801–2820.
26. Bourgeois JP, Goldman-Rakic PS, Rakic P (1994) Synaptogenesis in the prefrontal cortex of rhesus monkeys. *Cereb Cortex* 4: 78–96.
27. Zecevic N, Bourgeois JP, Rakic P (1989) Changes in synaptic density in motor cortex of rhesus monkey during fetal and postnatal life. *Develop Brain Res* 50: 11–32.
28. Zecevic N, Rakic P (1991) Synaptogenesis in monkey somatosensory cortex. *Cereb Cortex* 1: 510–523.
29. Huttenlocher PR, Dabholkar AS (1997) Regional differences in synaptogenesis in human cerebral cortex. *J Comp Neurol* 387: 167–178.
30. Chugani HT (1998) A critical period of brain development: Studies of cerebral glucose utilization with PET. *Preventive Medicine* 27: 184–188.
31. Attwell D, Laughlin SB (2001) An energy budget for signaling in the gray matter of the brain. *J Cereb Blood Flow Metab* 21: 1133–1145.
32. Lennie P (2003) The cost of cortical computation. *Curr Biol* 13: 493–497.
33. Karbowski J (2009) Thermodynamic constraints on neural dimensions, firing rates, brain temperature and size. *J Comput Neurosci* 27: 415–436.
34. Nehlig A, de Vasconcelos AP, Boyet S (1988) Quantitative autoradiographic measurement of local cerebral glucose utilization in freely moving rats during postnatal development. *J Neurosci* 8: 2321–2333.
35. Chugani HT, Hovda DA, Villablanca JR, Phelps ME, Xu WF (1991) Metabolic maturation of the brain: A study of local cerebral glucose utilization in the developing cat. *J Cereb Blood Flow Metab* 11: 35–47.
36. Moore AH, Hovda DA, Cherry SR, Villablanca JP, Pollack DB, et al. (2000) Dynamic changes in cerebral glucose metabolism in conscious infant monkeys during the first year of life as measured by positron emission tomography. *Develop Brain Res* 120: 141–150.
37. Jacobs B, Chugani HT, Allada V, Chen S, Phelps ME, et al. (1995) Developmental changes in brain metabolism in sedated rhesus macaques and vervet monkeys revealed by positron emission tomography. *Cereb Cortex* 3: 222–233.
38. Noda A, Ohba H, Kakiuchi T, Futatsubashi M, Tsukada H, et al. (2002) Age-related changes in cerebral blood flow and glucose metabolism in conscious rhesus monkeys. *Brain Res* 936: 76–81.
39. Kinnala A, Suhonen-Polvi H, Aarimaa T, Kero P, Korvenranta H, et al. (1996) Cerebral metabolic rate for glucose during the first six months of life: an FDG positron emission tomography study. *Archives of Disease in Childhood* 74: F153–F157.
40. Bolshakov VY, Siegelbaum SA (1995) Regulation of hippocampal transmitter release during development and long-term potentiation. *Science* 269: 1730–1734.
41. Frick A, Feldmeyer D, Sakmann B (2007) Postnatal development of synaptic transmission in local networks of L5A pyramidal neurons in rat somatosensory cortex. *J Physiol* 585: 103–116.
42. Gonzalez-Burgos G, Kroener S, Zaitsev AV, Povysheva NV, Krimer LS, et al. (2008) Functional maturation of excitatory synapses in layer 3 pyramidal neurons during postnatal development of the primate prefrontal cortex. *Cereb Cortex* 18: 626–637.
43. Yoshimura Y, Kimura F, Tsumoto T (1999) Estimation of single channel conductance underlying synaptic transmission between pyramidal cells in the visual cortex. *Neuroscience* 88: 347–352.
44. Jahr CE, Stevens CF (1990) Voltage dependence of NMDA-activated macroscopic conductances predicted by single-channel kinetics. *J Neurosci* 10: 3178–3182.
45. Volgushev M, Kudryashov I, Chistiakova M, Mukovski M, Niesman J, et al. (2004) Probability of transmitter release at neocortical synapses at different temperatures. *J Neurophysiol* 92: 212–220.
46. Murthy VN, Schikorski T, Stevens CF, Zhu Y (2001) Inactivity produces increases in neurotransmitter release and synapse size. *Neuron* 32: 673–682.
47. Pakkenberg B, Gundersen HJ (1997) Neocortical neuron number in humans: effect of sex and age. *J Comp Neurol* 384: 312–320.
48. Sowell ER, Peterson BS, Thompson PM, Welcome SE, Henkenius AL, et al. (2003) Mapping cortical change across the human life span. *Nature Neurosci* 6: 309–315.
49. Herndon JG, Tigges J, Anderson DC, Klumpp SA, McClure HM (1999) Brain weight throughout the life span of the chimpanzee. *J Comp Neurol* 409: 567–572.
50. Giedd JN, Blumental J, Jeffries NO, Castellanos FX, Liu H, et al. (1999) Brain development during childhood and adolescence: a longitudinal MRI study. *Nature Neurosci* 2: 861–863.
51. Shaw P, Kabani NJ, Lerch JP, Eckstrand K, Lenroot R, et al. (2008) Neurodevelopmental trajectories of the human cerebral cortex. *J Neurosci* 28: 3586–3594.
52. Raznahan A, Shaw P, Lalonde F, Stockman M, Wallace GL, et al. (2011) How does your cortex grow? *J Neurosci* 31: 7174–7177.
53. Rolfe DFS, Brown GC (1997) Cellular energy utilization and molecular origin of standard metabolic rate in mammals. *Physiol Rev* 77: 731–758.
54. Lüscher C, Nicoll RA, Malenka RC, Muller D (2000) Synaptic plasticity and dynamic modulation of the postsynaptic membrane. *Nature Neurosci* 3: 545–550.
55. Montgomery MJ, Madison DV (2004) Discrete synaptic states define a major mechanism of synaptic plasticity. *Trends Neurosci* 27: 744–750.
56. Braitenberg V, Schüz A (1998) *Cortex: Statistics and Geometry of Neuronal Connectivity*. Berlin: Springer.
57. DeFelipe J, Alonso-Nanclares L, Avellano J (2002) Microstructure of the neocortex: Comparative aspects. *J Neurocytol* 31: 299–316.
58. Herculano-Houzel S (2011) Scaling of brain metabolism with a fixed energy budget per neuron: Implications for neuronal activity, plasticity, and evolution. *PLoS ONE* 6: e17514.
59. Karbowski J (2011) Scaling of brain metabolism and blood flow in relation to capillary and neural scaling. *PLoS ONE* 6: e26709.
60. Herculano-Houzel S, Mota B, Lent R (2006) Cellular scaling rules for rodent brains. *Proc Natl Acad Sci USA* 103: 12138–12143.
61. Herculano-Houzel S, Collins CE, Wong P, Kaas JH (2007) Cellular scaling rules for primate brains. *Proc Natl Acad Sci USA* 104: 3562–3567.
62. Mitchison G (1992) Axonal trees and cortical architecture. *Trends Neurosci* 15: 122–126.
63. Cherniak C (1994) Component placement optimization in the brain. *J Neuroscience* 14: 2418–2427.
64. Wen Q, Chklovskii DB (2005) Segregation of the brain into gray and white matter: A design minimizing conduction delays. *PLoS Comput Biol* 1: e78.
65. Kaiser M, Hilgetag CC (2006) Nonoptimal component placement, but short processing paths, due to long-distance projections in neural systems. *PLoS Comput Biol* 2: e95.
66. Turrigiano GG, Leslie KR, Desai NS, Rutherford LC, Nelson SB (1998) Activity-dependent scaling of quantal amplitude in neocortical neurons. *Nature* 391: 892–896.
67. Turrigiano GG, Nelson SB (2004) Homeostatic plasticity in the developing nervous system. *Nature Rev Neurosci* 5: 97–107.
68. Zito K, Svoboda K (2002) Activity-dependent synaptogenesis in the adult mammalian cortex. *Neuron* 35: 1015–1017.
69. van Ooyen A, van Pelt J (1994) Activity-dependent outgrowth of neurons and overshoot phenomena in developing neural networks. *J Theor Biol* 167: 27–43.
70. McGlashan TH, Hoffman RE (2000) Schizophrenia as a disorder of developmentally reduced synaptic connectivity. *Arch Gen Psychiatry* 57: 637–648.
71. Geschwind DH, Levitt P (2007) Autism spectrum disorders: developmental disconnection syndromes. *Curr Opin Neurobiol* 17: 103–111.
72. Erecinska M, Silver IA (1989) ATP and brain function. *J Cereb Blood Flow Metab* 9: 2–19.
73. Ames III A (2000) CNS energy metabolism as related to function. *Brain Research Reviews* 34: 42–68.

74. Burnashev N, Zhou Z, Neher E, Sakmann B (1995) Fractional calcium currents through recombinant glutamate receptor channels of the NMDA, AMPA, and kainate receptor subtypes. *J Physiol* 485: 403–418.
75. Brunel N (2000) Dynamics of sparsely connected networks of excitatory and inhibitory spiking neurons. *J Comput Neurosci* 8: 183–208.